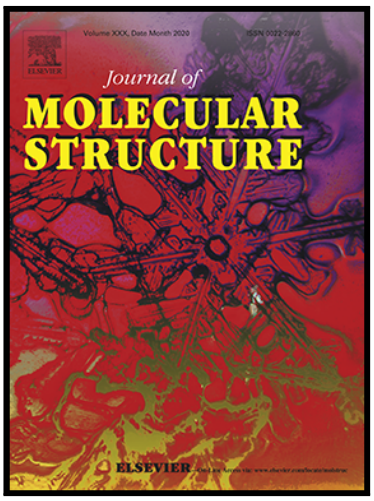

Highly functionalized N-1-(2-pyridinylmethyl)-3,5-bis[(E)-arylmethylidene]tetrahydro-4(1H)-pyridinones: Synthesis, characterization, crystal structure and DFT studies

Dhaifallah M. Al-thamili , Abdulrahman I. Almansour , Natarajan Arumugam , Sevgi Kansız , Necmi Dege , Saied M. Soliman , Mohammad Azam , Raju Suresh Kumar

PII: S0022-2860(20)31265-5
DOI: https://doi.org/10.1016/j.molstruc.2020.128940
Reference: MOLSTR 128940

To appear in: *Journal of Molecular Structure*

Received date: 6 June 2020
Revised date: 18 July 2020
Accepted date: 19 July 2020

Please cite this article as: Dhaifallah M. Al-thamili , Abdulrahman I. Almansour , Natarajan Arumugam , Sevgi Kansız , Necmi Dege , Saied M. Soliman , Mohammad Azam , Raju Suresh Kumar , Highly functionalized N-1-(2-pyridinylmethyl)-3,5-bis[(E)-arylmethylidene]tetrahydro-4(1H)-pyridinones: Synthesis, characterization, crystal structure and DFT studies, *Journal of Molecular Structure* (2020), doi: https://doi.org/10.1016/j.molstruc.2020.128940

Highlights

- Highly functionalized α,β-unsaturated carbonyl compounds were achieved in good yields.
- Molecular structure was elucidated by NMR spectroscopic and X-ray crystallographic studies.
- Molecular packing was performed to determine different intermolecular contacts using Hirshfeld analysis.
- DFT calculations are used in order to predict the electronic properties of studied compounds.

Highly functionalized *N*-1-(2-pyridinylmethyl)-3,5-bis[(*E*)-arylmethylidene]tetrahydro-4(1*H*)-pyridinones: Synthesis, characterization, crystal structure and DFT studies

Dhaifallah M. Al-thamili,[1] Abdulrahman I. Almansour,[1] Natarajan Arumugam,[1] Sevgi Kansız,[2] Necmi Dege,[3] Saied M. Soliman[4], Mohammad Azam[1] and Raju Suresh Kumar[1,*]

[1]*Department of Chemistry, College of Science, King Saud University, P.O. Box 2455, Riyadh 11451, Saudi Arabia*
[2]*Department of Fundamental Sciences, Faculty of Engineering, Samsun University, Samsun, 55420, Turkey*
[3]*Department of Physics, Faculty of Arts and Sciences, Ondokuz Mayıs University, Samsun, 55139, Turkey*
[4]*Department of Chemistry, Faculty of Science, Alexandria University, P.O. Box 426, Ibrahimia, Alexandria 21321, Egypt*

Abstract

Highly functionalized *N*-1-(2-pyridinylmethyl)-3,5-bis[(*E*)-methoxy/fluorophenylmethylidene]-tetrahydro-4(1*H*)-pyridinones (**5a** and **5b**) have been synthesized in good yields. The molecular structure of the synthesized compounds was elucidated by NMR spectroscopy and further confirmed by single crystal X-ray crystallographic studies. The Hirshfeld analysis reveals that the molecular packing of **5a** is mainly controlled by N...H (4.9%), C...H (30.6%) and H...H (52.4%) contacts whereas the molecules are packed by strong F...H (16.8-16.9 %), N...H (5.4%) and O...H (5.2-5.4%) as well as weak C...C (3.9-4.5%), H...H (39.7-39.9%) and C...H (24.8-25.8%) contacts in **5b**. DFT calculations are used in order to predict the electronic properties of studied compounds. The NMR data obtained experimentally correlated well with the calculated findings.

Keywords: Functionalized α,β-unsaturated ketones; X-ray analysis; Hirshfeld; DFT studies.

*Corresponding authors: Email: sraju@ksu.edu.sa; drrajusureshkumar@gmail.com (Suresh Kumar R).

1. Introduction

Heterocyclic compounds are of central importance to biological processes and are prevalent as natural products. Heterocyclic hybrids designed and synthesized by organic chemists are used as pharmaceuticals and play vital roles in human life. The noteworthy aptitude of heterocyclic nuclei to serve both as biomimetics and active pharmacophores has fundamentally contributed to their unique value as traditional key elements of several drugs [1,2].

Compounds possessing α,β-unsaturated carbonyl groups are the central core of several biologically active compounds displaying fascinating biological properties [3-6]. Conjugated unsaturated ketones have the capacity to interact favorably with thiols in contrast to amino and hydroxyl groups present in nucleic acids. Thus, the genotoxic properties exhibited by various alkylating agents in cancer chemotherapy may well be absent in conjugated enones [7]. Many lead compounds have been developed due to their diverse biological properties and hence compounds possessing α,β-unsaturated carbonyl groups have become a tool of choice both in academia and industry.

Anticancer drug research reveals that piperidinone derivatives embedded with α,β-unsaturated group exhibit potent and promising activity against cancer cell lines [8,9]. Compounds containing two or more alkylation sites demonstrated selective toxicity towards neoplastic cells in contrast to the corresponding normal tissues [10] and hence compounds with two sites for thiolation are of paramount importance. It is also believed that the piperidone derivatives with more unsaturated groups would have greater potency than the ones with less and/or no unsaturated groups since steric impedance to attack by thiols would be less in the case of former [9]. In particular, the 3,5-bis(arylidene)-4-piperidones demonstrate IC_{50} values in the low micromolar to submicromolar range towards a number of cell lines. It is reported that these compounds show both antitumor and fluorescent properties, and draw extensive attention as potential fluorescent antitumor drug candidates [11,12]. Therefore, the development of series of target compounds seemed to be judicious.

In continuation of our earlier research findings in the construction and/or biological screening of novel heterocycles possessing piperidone structural motif [13-20], here in we propose the synthesis of novel α,β-unsaturated carbonyl groups engrafted *N*-substituted piperidones. The structural elucidation of the synthesized compounds was performed by

spectroscopic techniques and single crystal X-ray crystallography. Molecular packing was done to determine the different intermolecular contacts in the crystal structure using Hirshfeld topology analysis. Furthermore, DFT calculations were also performed to evaluate the structural aspects and to assign the NMR chemical shifts of these compounds. In addition, the electronic properties and reactivity descriptors were also calculated and compared.

2. Experimental

2.1. Chemistry

All reagents and solvents were purchased from commercial suppliers and used without further purification. Reactions were monitored by thin-layer chromatography (TLC) on silica gel. Melting points were taken using open capillary tubes and are uncorrected. ^{1}H, ^{13}C and two-dimensional NMR spectra were recorded on a Jeol 500 MHz instrument in $CDCl_3$ using Tetramethylsilane (TMS) as internal standard. Standard Jeol software was used throughout. Chemical shifts are given in parts per million (δ-scale) and the coupling constants are given in Hertz. FT-IR spectra were recorded on a Perkin Elmer system 2000 FT-IR instrument (KBr). Mass spectra were recorded on a DART-ToF-MS mass spectrometer. X-ray data set were collected from STOE IPDS 2 Diffractometer and SHELXL2018/3 (Sheldrick, 2018) Program(s) was used to refine structures.

2.2. General procedure for the synthesis of N-1-(2-pyridinylmethyl)-3,5-bis[(E)-arylmethylidene]tetrahydro-4(1H)-pyridinones ***5(a,b)***

A mixture of 3,5-bis[(*E*)-arylmethylidene]tetrahydro-4(1*H*)-pyridinones **(3)** (1mmol) and K_2CO_3 (3 mmol) in acetonitrile (20 mL) was stirred at room temperature for 30 min. Then 2-(chloromethyl)pyridine hydrochloride **4** (1.1 mmol) dissolved in acetonitrile (5 mL) was added. The mixture was stirred and refluxed until the consumption of the starting materials was complete. The reaction progress was monitored by TLC. After the reaction was complete (24 h), the mixture was cooled to room temperature, the inorganic salts were filtered off on sintered glass filter and washed with $CHCl_3$ (10 mL). The filtrate was evaporated, and the residue was partitioned between $CHCl_3$ (20 mL) and water (10 mL). The organic phase was separated, and the aqueous phase was washed with $CHCl_3$ (20mL). The combined organic phase was dried (Na_2SO_4), filtered, and evaporated. The crude product was purified by crystallization using acetonitrile to afford compound **5**.

*2.2.1. N-1-(2-Pyridinylmethyl)-3,5-bis[(E)-(2-methoxylphenyl)methylidene]tetrahydro-4(1H)-pyridinone (**5a**)*

Obtained as yellow solid, Yield = 85 %; mp = 120-122 °C; IR (KBr): 1670, 1614, 1586 cm^{-1}; ^{1}H NMR (500 MHz, $CDCl_3$): δ_H 3.78 (s, 3H, OCH_3), 3.81 (s, 3H, OCH_3), 3.82-3.83 (m, 6H, 2'-CH_2, 6-CH_2' and 7'-CH_2), 6.86-6.90 (m, 4H, ArH), 7.02-7.12 (m, 3H, ArH), 7.23-7.29 (m, 3H, ArH), 7.43-7.46 (m, 1H, ArH), 8.06 (s, 2H, ArH), 8.44-8.45 (m, 1H, ArH). ^{13}C NMR (125 MHz, $CDCl_3$): δ_C 54.60, 55.19, 62.35, 110.37, 119.75, 121.78, 122.68, 124.06, 129.94, 130.11, 132.26, 132.90, 136.120, 148.80, 157.89, 158.08, 187.34. Mass: 427 [M^+]. Anal. calcd for $C_{27}H_{26}N_2O_3$: C, 76.03; H, 6.14; N, 6.57%; found: C, 76.24; H, 6.02; N, 6.70%.

*2.2.2. N-1-(2-Pyridinylmethyl)-3,5-bis[(E)-(4-fluorophenyl)methylidene]tetrahydro-4(1H)-pyridinone (**5b**)*

Obtained as yellow solid, Yield = 88 %; mp = 110–112 °C; IR (KBr): 1668, 1615, 1588 cm^{-1}; ^{1}H NMR (500 MHz, $CDCl_3$): δ_H 3.84-3.87 (m, 6H, 2'-CH_2, 6'-CH_2 and 7'-CH_2), 7.03-7.11 (m, 5H, ArH), 7.28-7.33 (m, 5H, ArH), 7.51-7.54 (m, 1H, ArH), 7.74 (s, 2H, ArH), 8.48-8.49 (m, 1H, ArH). ^{13}C NMR (125 MHz, $CDCl_3$): δ_C 54.73, 63.23, 115.60, 115.78, 122.35, 122.99, 131.23, 131.24, 132.30, 132.77, 135.36, 136.62, 149.16, 157.62, 161.86, 163.86, 187.19. Mass: 403 [M^+].

Anal. calcd for $C_{25}H_{20}F_2N_2O$: C, 74.61; H, 5.01; N, 6.96%; found: C, 74.77; H, 5.14; N, 6.85%.

2.3. X-Ray analysis

The diffraction intensity data of **5a** $C_{27}H_{26}N_2O_3$ and **5b** $C_{25}H_{20}F_2N_2O$ was obtained by using MoKα radiation with STOE IPDS 2 [21] diffractometer with graphite-monochromated MoKα radiation (λ = 0.71073 Å) at 296 K. In the data collection and reduction processes, X-AREA [21] and X-RED [21] programs were used, respectively. Crystal structure was resolved using SHELXT [22] software and refined with SHELXL [23] software using direct methods, which are included in the WinGX [24] program. The results were visualized using MERCURY [25] software. C–bonded hydrogen atoms were refined as riding model C—H = 0.93–0.97 Å.

Table 1. Crystal data and refinement details for **5a** and **5b**.

Crystal Data	**(5a)**	**(5b)**
Chemical Formula	$C_{27}H_{26}N_2O_3$	$C_{25}H_{20}F_2N_2O$

Formula weight (a.k.b.)	426.5	402.43
Temperature (K)	296	296
Crystal system	Monoclinic	Triclinic
Space group	$P2_1/c$	*P-1*
Unit cell parameters		
a, b, c (Å)	11.6907 (10), 21.5030 (11), 9.8644 (7)	9.1736 (15), 11.8482 (14), 19.097 (3)
β (˚)	112.987 (6)	91.293 (11), 93.917 (13), 90.250 (12)
Crystal size (mm)	0.75 × 0.42 × 0.15	0.42 × 0.29 × 0.16
Volume, V (Å^3)	2282.9 (3)	2070.2 (5)
Z	4	4
μ (mm^{-1})	0.08	0.09
F_{000}	904	840
Calculated density (Mg/m^3)	1.241	1.291
Data collection		
Diffractometer	STOE IPDS 2	STOE IPDS 2
Wavelength (Å)	0.71073	0.71073
θ range for data collection (˚)	1.9 ≤ θ ≤ 28.9	1.7 ≤ θ ≤ 28.3
Index ranges		
h_{min}, h_{max}	-10, 14	-10, 10
k_{min}, k_{max}	-26, 26	-14, 14
l_{min}, l_{max}	-12, 12	-22, 22
Measurement method	*ω* scan	*ω* scan
Reflections collected	11306	19859
Independent reflections	4403	7319
Observed reflections [I > 2σ(I)]	2218	2914
Absorption correction	Integration	Integration
T_{min}, T_{max}	0.957, 0.990	0.967, 0.994
R_{int}	0.075	0.101
Refinement		
Refinement method	SHELXL17/1	SHELXL17/1
Parameters	291	542
R[$F^2 > 2\sigma(F^2)$]	0.045	0.076
wR(F^2)	0.105	0.242
GooF = S	0.83	0.92
$\Delta\rho_{min}$, $\Delta\rho_{max}$ (e/Å^3)	-0.17, 0.14	-0.14, 0.21

2.4. Computational methods

The topology analyses of molecular packing were performed using Crystal Explorer 17.5 program [26]. Gaussian 09 software package [27,28] employing B3LYP/6-31G(d,p) method were used for geometry optimization. Natural charge calculations were performed using NBO 3.1 program as implemented in the Gaussian 09W [29]. The structure of both compounds was further optimized in solution using chloroform as solvent applying the self-consistent reaction filed (SCRF) method [30,31]. Then, the optimized structures were used to compute the NMR chemical shifts of the protons and carbons using GIAO method [32].

3. Results and discussion

3.1. Chemistry

The highly functionalized target compounds viz, *N*-1-(2-pyridinylmethyl)-3,5-bis[(*E*)-arylmethylidene]tetrahydro-4(1*H*)-pyridinones **5a** and **5b** were synthesized through the alkylation of compounds **3a** and **3b** with an equivalent amount of 2-(chloromethyl)pyridine hydrochloride in the presence of K_2CO_3 (Scheme 1). The synthesis of 3,5-bis[(*E*)-arylmethylidene]tetrahydro-4(1*H*)-pyridinones **3a** and **3b** was carried out according to the method reported by Dimmock *et al*. in acetic acid [33]. Initially, in order to optimize the reaction conditions, a representative reaction was performed with different solvents viz, dioxane, acetonitrile, dimethylformamide (DMF), methanol, ethanol and chloroform (Table 2). The reactions under dioxane, methanol, ethanol, dimethylformamide and chloroform afforded the product only in traces even after prolonged reaction times whereas the reaction in acetonitrile afforded the compound 5 in good yield. Hence, in a typical reaction, a mixture **3b** (1 mmol) and K_2CO_3 (3 mmol) in acetonitrile (20 mL) was stirred at room temperature for 30 min. Then 2-(chloromethyl)pyridine hydrochloride **4** (1 mmol) dissolved in acetonitrile (5 mL) was added. The reaction mixture was refluxed until the complete consumption of all the starting materials as confirmed by TLC analysis. The target α,β-unsaturated carbonyl compound **5b** was obtained in good yield. Subsequently, the other reaction was performed under this optimized reaction condition and resulted a good yield (85 %) of the compound **5a**.

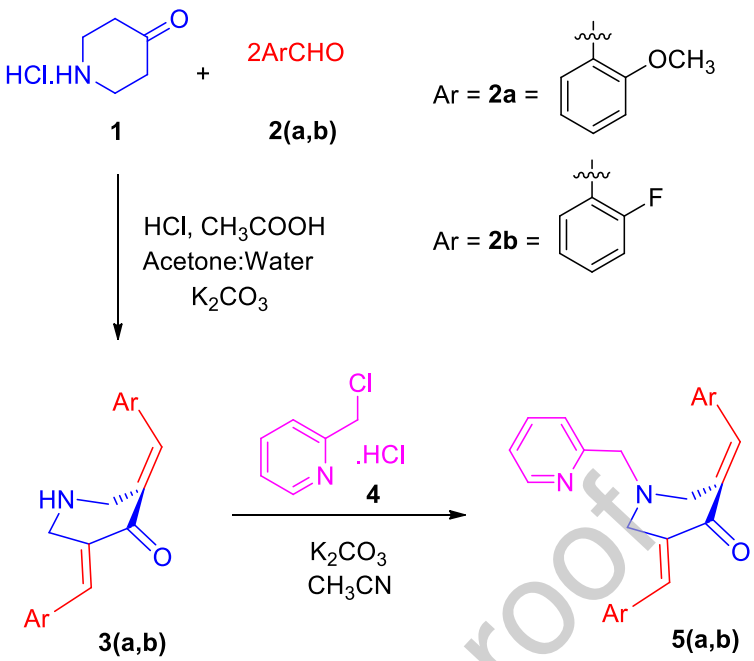

Scheme 1. Synthesis of *N*-1-(2-pyridinylmethyl)-3,5-bis[(*E*)-arylmethylidene]tetrahydro-4(1*H*)-pyridinones **5**.

Table 2. Solvent optimization for the synthesis of *N*-1-(2-pyridinylmethyl)-3,5-bis[(*E*)-aryl-methylidene]tetrahydro-4(1*H*)-pyridinones **5b**.

Entry	Solvents	Temp (°C)	Time (h)	Yield[a] (%)
1	Dioxane	100	12	b
2	Methanol	60	12	b
3	Ethanol	75	12	b
4	DMF	100	24	20
5	Chloroform	60	10	b
6	Acetonitrile	80	24	88

[a]Isolated yield
[b]No reaction

A careful structural elucidation of compounds **5**(**a,b**) was accomplished with the help of FT-IR, NMR spectroscopic and Mass spectrometry data. As an illustrative case, structural explanation of compound **5b** is discussed here. In the IR spectrum of **5b**, the main infrared

absorption peaks at υ_{max} 1668, 1615 and 1588 cm^{-1} are assigned to C=O and C=C groups. In its ^{1}H NMR spectrum the multiplet at 3.84-3.87 ppm is assigned to 7'-CH_2, 6'-CH_2 and 2'-CH_2 protons. The phenylmethylidene proton, H-8' appear as a singlet at 7.74 ppm. The aromatic protons appear as multiplets around 7.03-8.45 ppm. In the ^{13}C NMR spectrum, the carbon signals at 54.73 ppm and 63.23 ppm were due to C-2'/C-6' and C-7' respectively whilst the C-8' appeared at 149.16 ppm. The carbonyl carbon appears at 187.19 ppm and the aromatic carbons appeared at 115.60-163.86 ppm. The selected ^{1}H and ^{13}C chemical shifts of **5b** are shown in Figure 1. The presence of molecular ion peak at 403 [M^{+}] in the mass spectrum confirms the formation of **5b**. The structure of other dipolarophile **5a** was also established based on similar straightforward considerations.

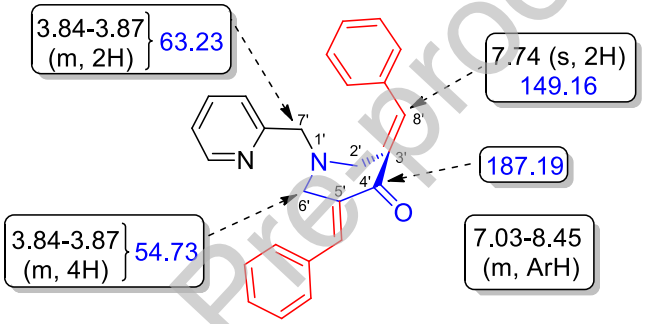

Figure 1. Selected ^{1}H and ^{13}C NMR chemical shifts of **5b**

3.2. X-ray crystallography

The structure of the compounds **5a** and **5b** was further confirmed by the single crystal X-ray analyses of [34]. The common moiety for **5a** and **5b** is 1-(pyridin-2-ylmethyl)piperidin-4-one. Figures 2 and 3 show the asymmetric unit of **5a** and **5b** respectively. Table 1 summarizes the experimental details (crystal data, data collection and structure refinement). Compound **5a** has one independent molecule in the asymmetric unit while **5b** contains two independent organic molecules and are not planar. In **5b**, the C2–C7 benzene ring is inclined to the piperidine ring by 24.61(12)˚, while the corresponding angle for C14–C19 benzene ring is 54.35(9)˚ in **5a**. The piperidine and pyridine rings were twisted with respect to each other, making a dihedral angle of 77.27(7)˚. In molecule 1, (the molecule with atom numbering, O1, N1, N2, F1 and F2) the C13–C18 fluorobenzene ring is inclined to the C20–C25 fluorobenzene ring by 27.8 (3)˚, while the corresponding angle in molecule 2 is 26.1 (3)˚ in **5b**. The piperidine ring is inclined to the plane

of the pyridine ring, the dihedral angle being 73.9 (2)˚ in molecule 1. For molecule 2, (the molecule with atom numbering, O2, N3, N4, F3 and F4) the piperidine and pyridine rings are twisted with respect to each other, making a dihedral angle of 74.2 (2)˚. A view of inverted molecule 1 (red) on molecule 2 (blue), the molecule overlay illustrates the difference in the conformations of the two molecules in Figure 4. The molecular structure is stabilized by the intermolecular C—H···N hydrogen bond along the *b*-axis direction in **5a** whilst the molecules in **5b** are linked by a pair of C—H···F hydrogen bonds forming inversion dimers with an $R_2^2(8)$ ring motif (Figures 5 and 6, and Table 3). The dimers are linked by C—H···O hydrogen bonds forming chains along the *c*-axis direction. The chains are linked by very weak π-stacking interactions, forming a three-dimensional network. In the methoxy groups in **5a**, the C1—O1 and C20—O3 bond distances are essentially equivalent, 1.423(2) Å and 1.424(3) Å, respectively. The C11—O2 (in **5a**), C9—O1 and C34—O2 (in **5b**) bond lengths are typical of double bonds. The detailed geometric parameters of **5a** and **5b** are given in Tables 4 and 5.

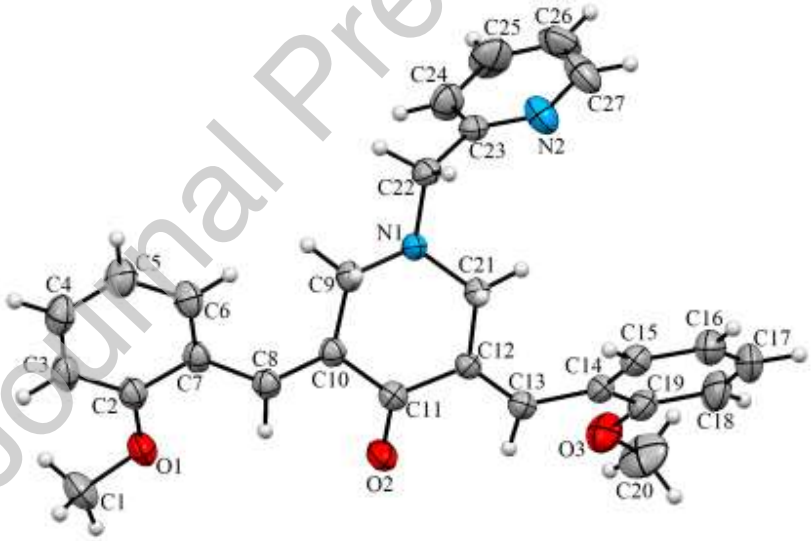

Figure 2. ORTEP diagram of **5a**, showing the atomic numbering and 30% probability displacement ellipsoids.

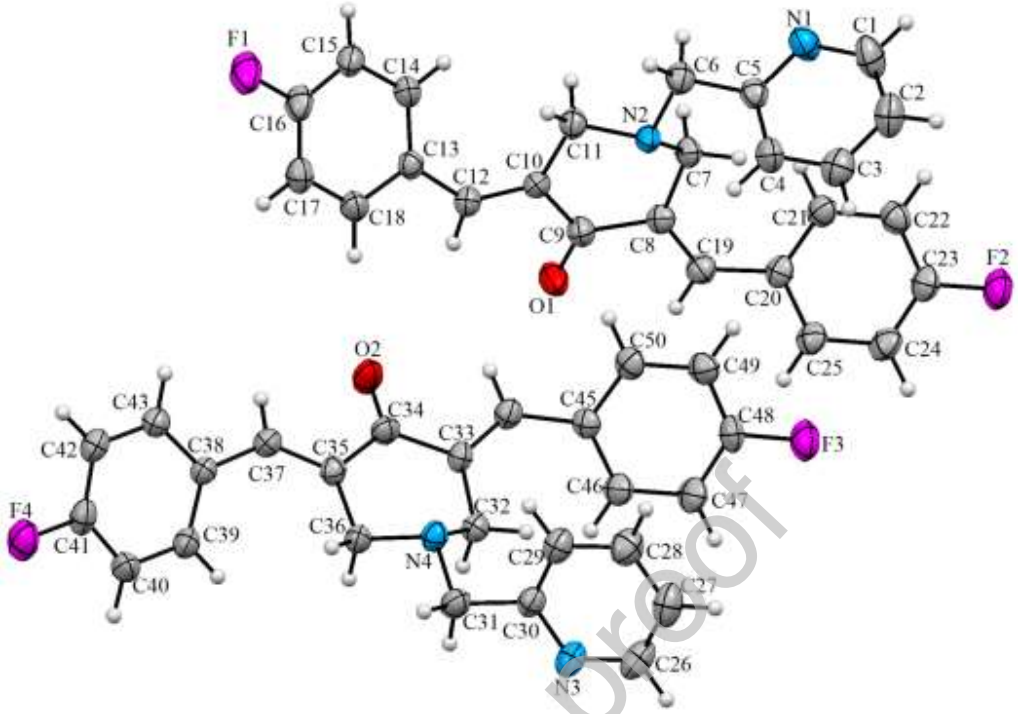

Figure 3. ORTEP diagram of **5b**, with the labelling scheme and 30% probability ellipsoids.

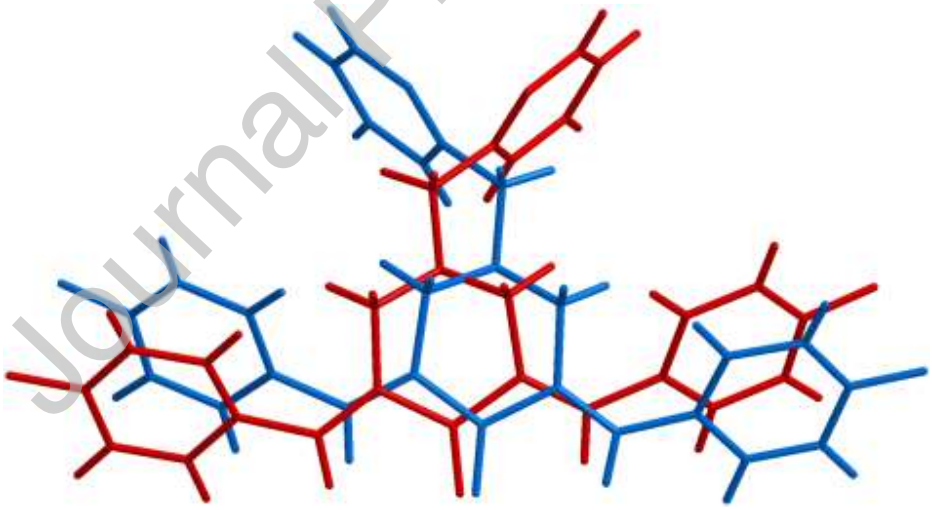

Figure 4. A molecular overlap view of inverted molecule 1 (red) on molecule 2 (blue) in **5b**.

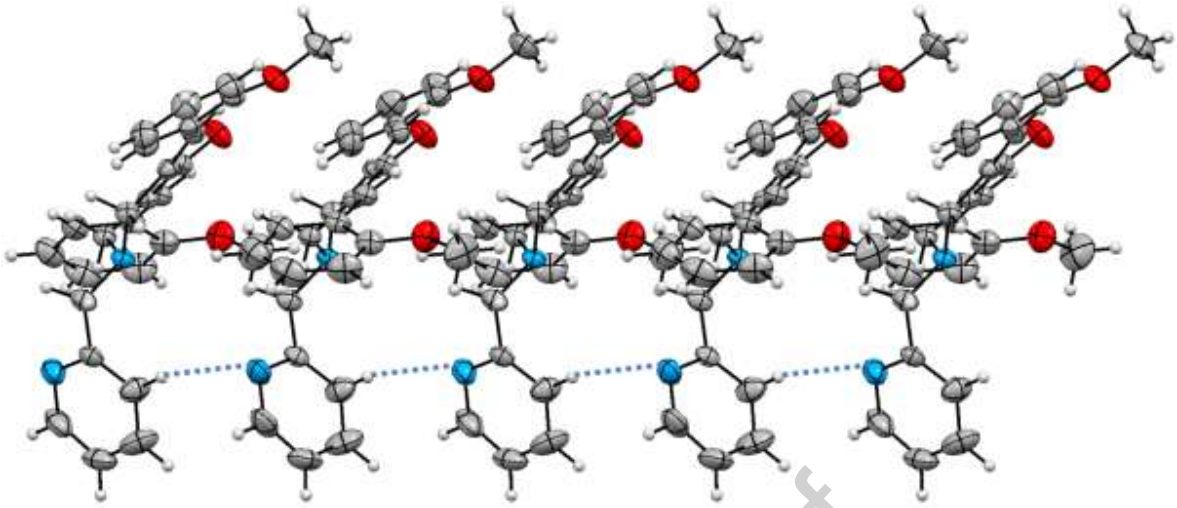

Figure 5. A partial view of the crystal packing of **5a** along the *b*-axis direction. Blue dashed lines denote the intermolecular C24—H24···N2 hydrogen bonds.

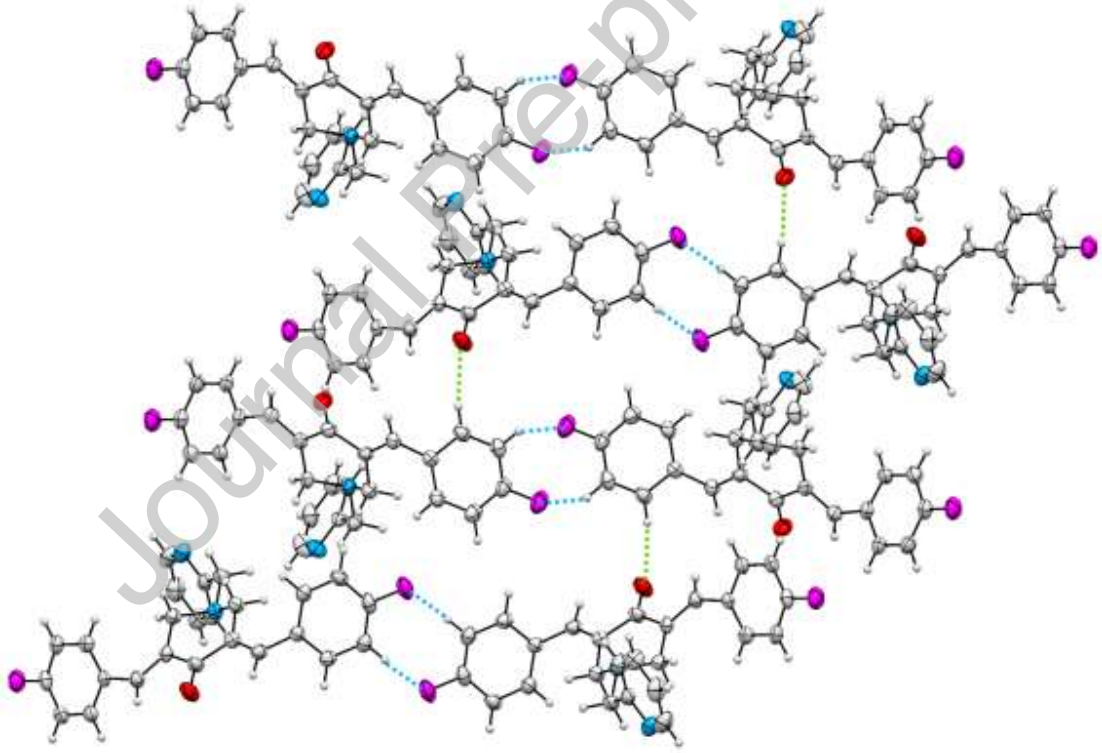

Figure 6. A partial view of the crystal packing of **5b** along the *c*-axis direction. Blue dashed lines denote the intermolecular C—H···F hydrogen bonds and green ones denote C—H···O hydrogen bonds.

Table 3. Hydrogen-bond geometries for **5a** and **5b** (Å, ˚).

D─H···A	*D*─H	H···A	*D*···A	*D*─H···A
(5a)				
C24─H24···N2^{i}	0.93	2.68	3.563 (3)	159
(5b)				
C42─H42···F4^{ii}	0.93	2.60	3.440 (8)	150
C29─H29···F3^{iii}	0.93	2.55	3.418 (9)	156
C17─H17···F1^{iv}	0.93	2.62	3.322 (9)	133
C4─H4···F2^{iii}	0.93	2.57	3.432 (9)	155
C18─H18···O2^{iii}	0.93	2.32	3.2058 (9)	158
C43─H43···O1^{v}	0.93	2.32	3.2210 (8)	162

Symmetry codes: (i) *x*, −*y*+1/2, *z*+1/2, (ii) −*x*−1, −*y*+1, −*z*+2; (iii) *x*−1, *y*, *z*; (iv) −*x*, −*y*, −*z*+2; (v) *x*+1, *y*+1, *z*.

Table 4. Selected geometric parameters for **5a** (Å, ˚).

Geometric Parameters	**X–Ray**
C1─O1	1.423 (2)
C2─O1	1.360 (2)
C11─O2	1.224 (2)
C19─O3	1.358 (3)
C20─O3	1.424 (3)
C9─N1	1.461 (2)
C21─N1	1.460 (2)
C22─N1	1.472 (2)
C23─N2	1.327 (2)
C27─N2	1.337 (3)
C22─C23	1.498 (3)
C12─C13	1.333 (2)
C13─C14	1.468 (3)
C7─C8	1.460 (3)
C8─C10	1.344 (3)
C1─O1─C2	119.1 (2)
C10─C11─O2	121.0 (2)
C12─C11─O2	121.0 (2)
C19─O3─C20	118.6 (2)
C9─N1─C21	109.7 (2)
C23─C22─N1	113.0 (2)
C23─N2─C27	116.8 (2)
C12─C13─C14	128.0 (2)

Table 5. Selected geometric parameters for **5b** (Å, ˚).

Geometric Parameters	**X–Ray**
C9─O1	1.222 (8)
C34─O2	1.213 (7)
C1─N1	1.330 (10)
C5─N1	1.338 (8)
C6─N2	1.462 (8)
C7─N2	1.472 (7)
C11─N2	1.455 (8)
C26─N3	1.339 (11)
C30─N3	1.329 (8)
C31─N4	1.472 (8)
C32─N4	1.452 (8)
C36─N4	1.450 (8)
C16─F1	1.350 (8)
C23─F2	1.360 (8)
C48─F3	1.372 (7)
C41─F4	1.368 (7)
C1─N1─C5	117.2 (7)
C6─N2─C7	109.1 (5)
C26─N3─C30	115.7 (7)
C31─N4─C32	109.8 (5)
C17─C16─F1	119.1 (7)
C22─C23─F2	118.0 (8)
C47─C48─F3	117.1 (7)
C41─C42─F4	118.1 (6)

3.3. Analysis of molecular packing

We employed Hirshfeld surface analysis to compare quantitatively the different intermolecular interactions affecting the molecular packing in the studied compounds (Figure 7). Full Hirshfeld surfaces are given in Figures S5 and S6 (*Supplementary data*). The molecular packing of **5a** is mainly controlled by relatively strong N...H (4.9%), C...H (30.6%) and H...H (52.4%) interactions. The corresponding fingerprint plots and decomposed d_{norm} maps for these interactions are shown in Figure 8. The N2...H24 (2.537 Å), C25...H20A (2.755 Å) and H18...H22B (2.139 Å), are the shortest contacts. The results also indicated the presence of some weak O...H (9.7%) contacts, all corresponding to C-H...O interactions. On other hand, the molecules of **5b** are packed by strong F...H (16.8-16.9 %), N...H (5.4%) and O...H (5.2-5.4%) interactions as well as weak C...C (3.9-4.5%), H...H (39.7-39.9%) and C...H (24.8-25.8%)

contacts. The crystal structure of this compound comprised two molecules per asymmetric unit, hence there are two results for each interaction in **5b**. Presentation of the decomposed d_{norm} maps for F...H, N...H and O...H interactions are shown in Figure 9 while the corresponding fingerprint plots are shown in Figure 10. The F4…H42 (2.469 Å), F3…H29 (2.41 Å), N1…H47 (2.615 Å), C42…C44 (3.375 Å), O1…H43 (2.18 Å) and O2…H18 (2.182 Å) are the shortest contacts where all appeared as red spots in the d_{norm} maps and sharp spikes in the fingerprint plots.

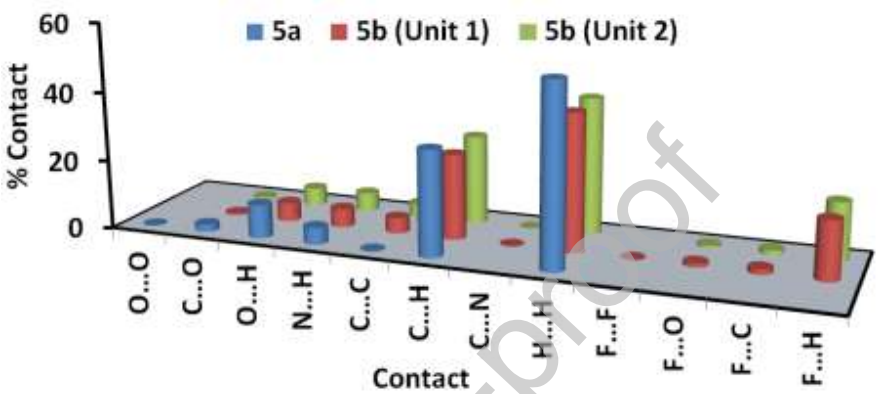

Figure 7. Summary of the intermolecular interactions and their percentages in the crystal structure of the studied compounds. Units **1** and **2** for **5b** refer to molecular units with lower and higher atom numbering respectively.

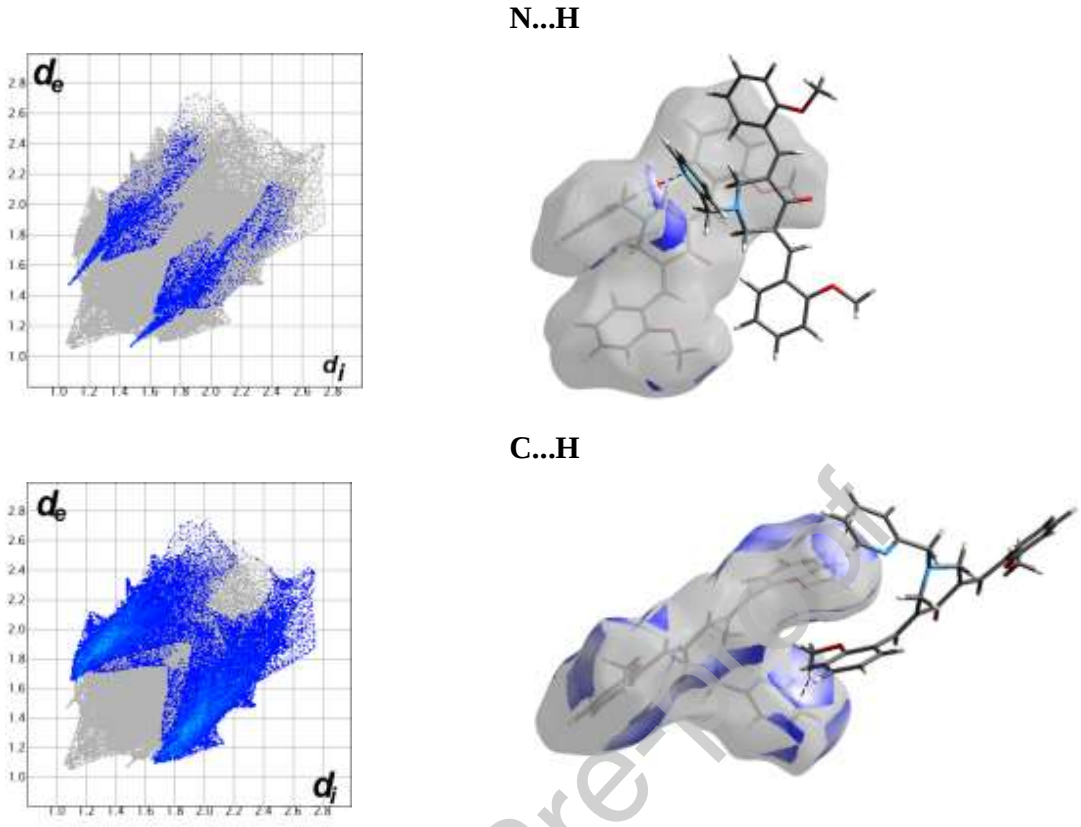

Figure 8. The decomposed fingerprint plots and d_{norm} maps of the N...H and C...H interactions in **5a**.

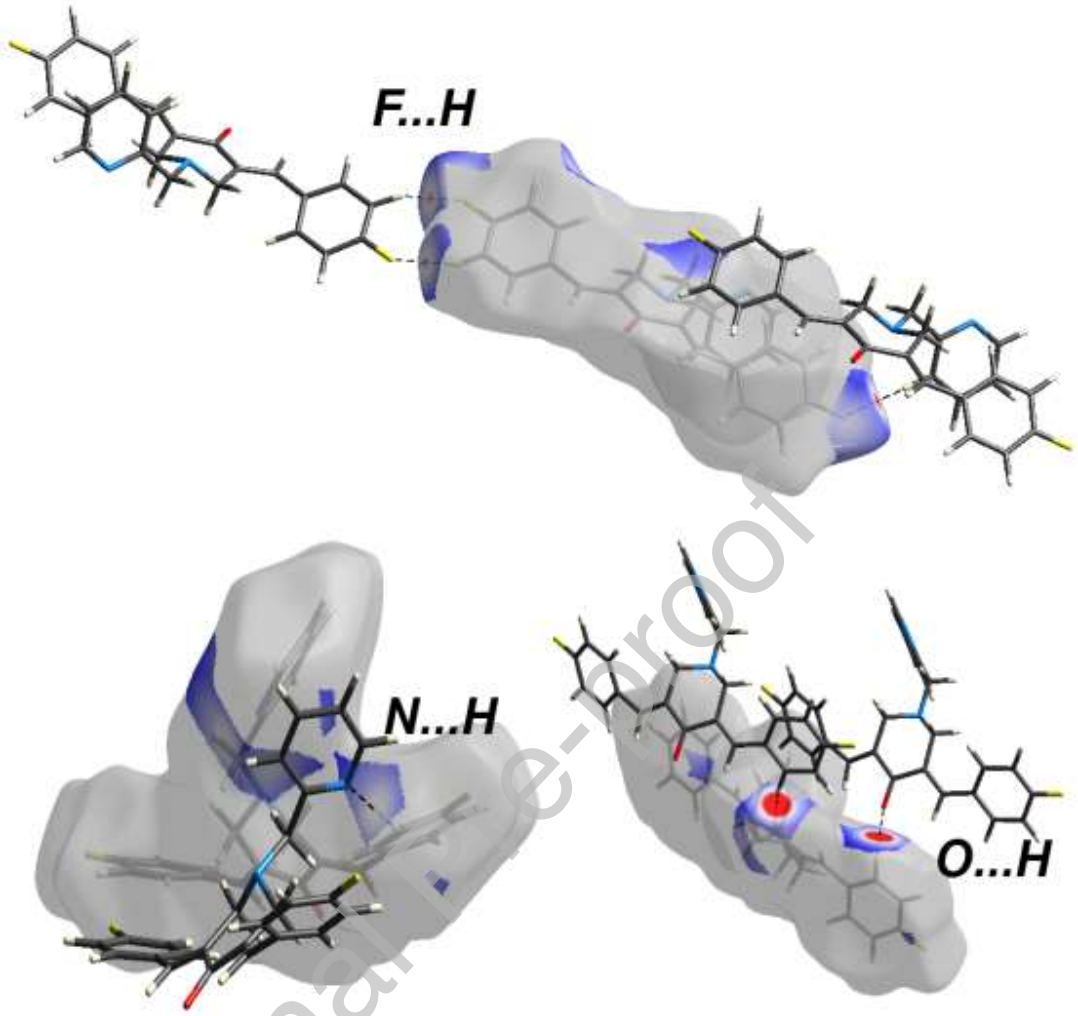

Figure 9. The decomposed d_{norm} maps of the F...H, N...H and O...H interactions in **5b**.

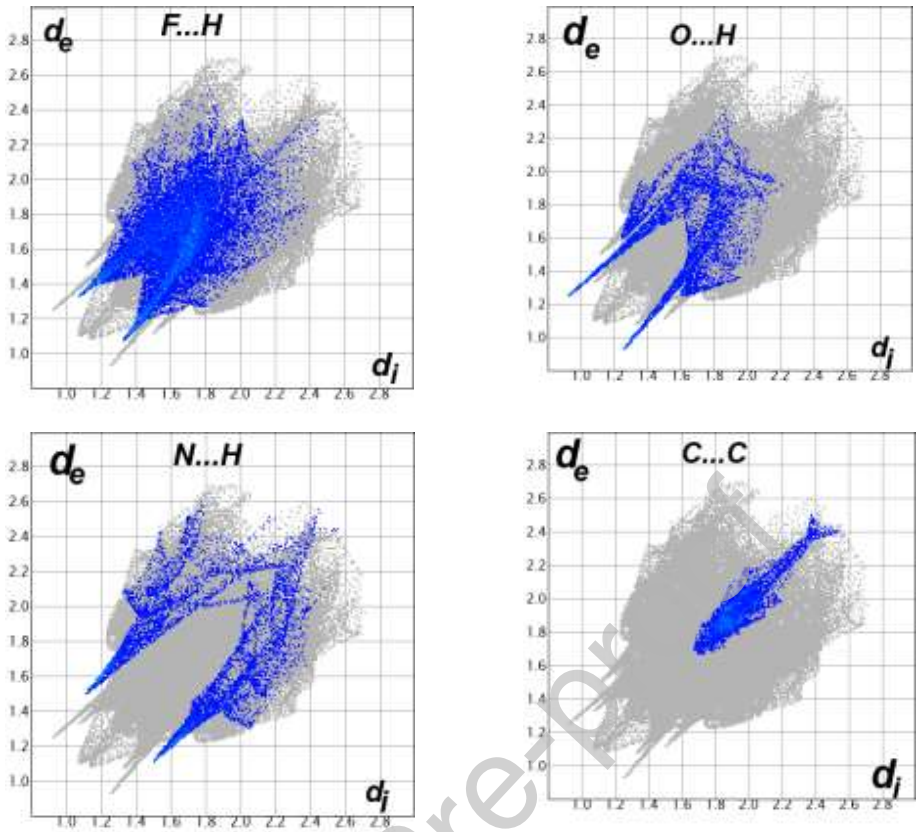

Figure 10. The decomposed fingerprint plots of the F...H, N...H, O...H and C...C interactions in **5b**.

3.4. DFT studies

Geometric parameters

The structures of **5a** and **5b** were optimized using B3LYP/6-31G(d,p) method. The calculated structures matched well with the experimental X-ray structures of the studied compounds as shown in Figure 11. The correlations between the calculated and experimental bond distances are 0.9613 and 0.9294 for **5a** and **5b**, respectively (Figure 12). Full geometric parameters were collected in Tables S1 and S2 (Supplementary data). The calculated dipole moment values are 2.125 and 1.578 Debye, respectively indicating the higher polarity of **5a** which contains methoxy groups as substituent than **5b** with the fluoro substituent. The reactivity indices [35-43] of both compounds such as ionization potential (I), electron affinity (A), chemical potential (μ), hardness (η), softness (S), and electrophilicity (ω) indices were calculated

based on the HOMO and LUMO energies and were found very close to each other (Table 6). The HOMO-LUMO energy gap is higher for **5b** (3.9307 eV) than **5a** (3.8061 eV). Hence, the former has slightly higher stability towards electron transfer than the latter. Compound **5b** has higher ionization potential and hence higher resistance towards oxidation than **5a**. Furthermore, high electron affinity for **5b** suggests its higher ability to gain electron than **5a**. On other hand, its electrophilic character as indicated from the electrophilicity index (ω) is higher than **5a**.

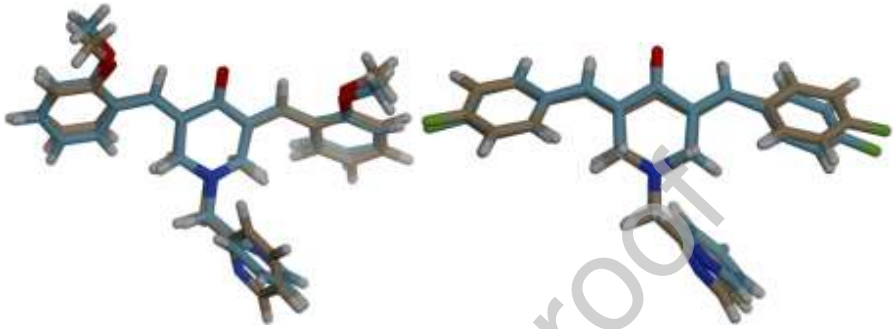

5a **5b**

Figure 11. Structure matches of the optimized and calculated structures of the studied organic compounds.

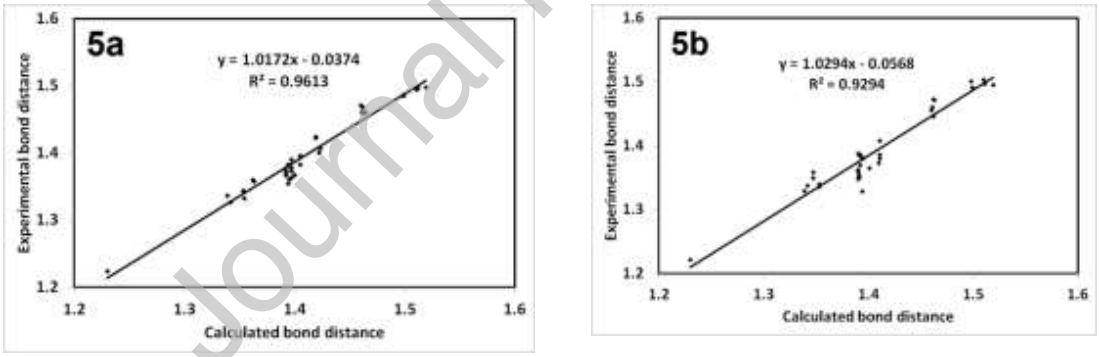

Figure 12. Correlations between calculated and experimental bond distances.

Table 6 HOMO and LUMO energies and the reactivity descriptors of **5a** and **5b**.

Parameter	**5a**	**5b**
HOMO	-5.6622	-6.1485
LUMO	-1.8561	-2.2177
I	5.6622	6.1485
A	1.8561	2.2177
η	3.8061	3.9307
μ	-3.7591	-4.1831
S	0.2627	0.2544
Ω	1.8564	2.2258

The natural charge distribution at different atomic sites were calculated and listed in Table S3 (*Supplementary data*). The O-atom of the carbonyl group in both compounds has the most negative charge. The natural charges at the carbonyl oxygen atom of **5a** and **5b** are -0.5753 and -0.5769 e, respectively. In contrast, the carbonyl carbon atoms have the highest positive charge in both the compounds. The natural charges at these atomic sites are 0.5251 and 0.5254 e for **5a** and **5b**, respectively. The variable charge distributions at the different atomic sites are responsible for the polarity of the studied molecules. Molecular electrostatic potential (MEP) map showing the electron density distribution as well as the dipole moment vector are shown in Figure 13. Also, the distribution of the HOMO and LUMO orbitals are shown in the same illustration. The distribution of these molecular orbitals sheds the light on the way by which the electron transfer could takes place in the studied systems. The HOMO level is mainly located over the pyridine moiety in **5a**, while distributed over the pyridine and the two aryl moieties in **5b**. This is considered as the demand from which the electron transport occurs. The LUMO in both compounds is distributed over the pyridine and the two aryl moieties which is the demand to which the electron transfer. The energy of these intramolecular charge transfer processes are 3.806 and 3.931 eV for compounds **5a** and **5b**, respectively.

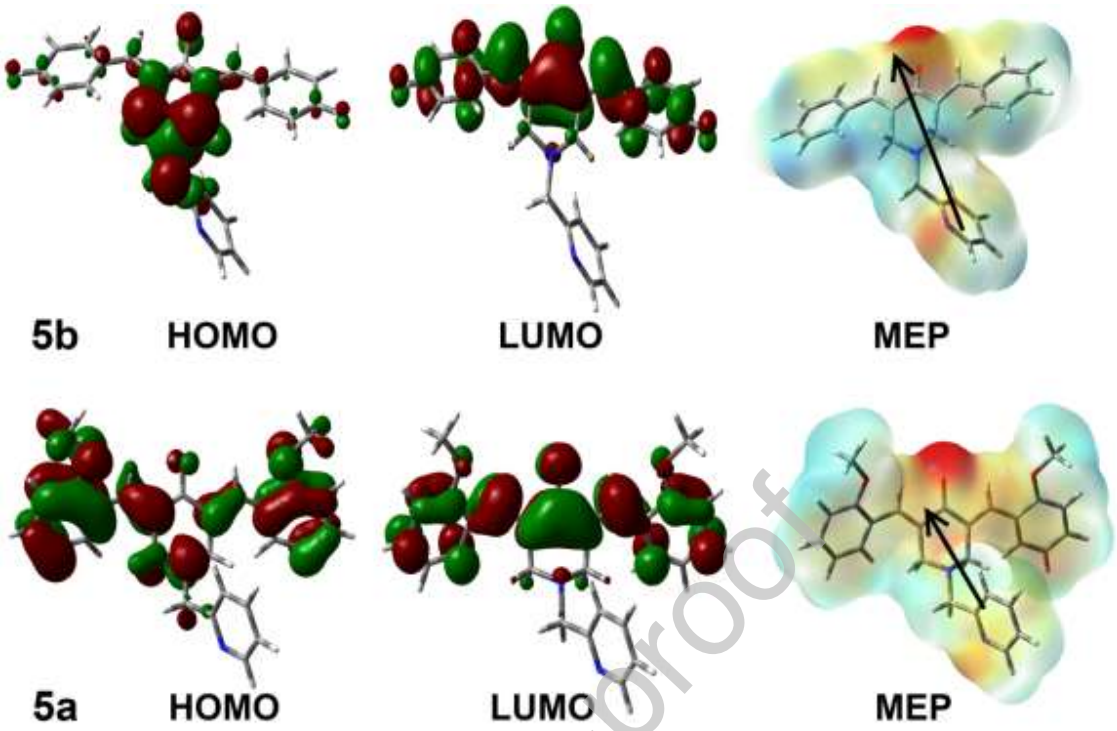

Figure 13. HOMO, LUMO and MEP with dipole moment vector of **5a** and **5b**.

3.5. NMR spectra

The ^{1}H and ^{13}C NMR chemical shift data were computed and the results are collected in Table S4 (*Supplementary data*). There are good agreements between the results obtained from the GIAO calculations with the experimental values measured in the same solvent where quite good correlations were obtained (Figure 14). As can be seen from this figure, the correlations coefficients (R^2) are in the range of 0.965-0.990 for ^{1}H NMR and 0.968-0.996 for ^{13}C NMR chemical shifts.

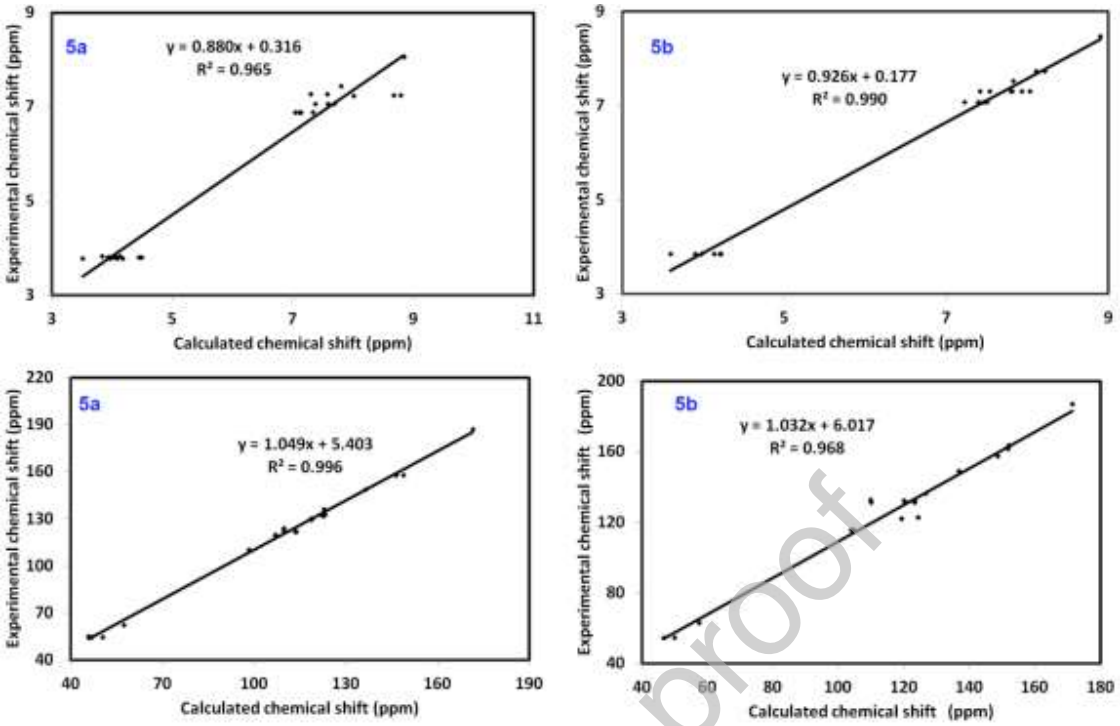

Figure 14. NMR chemical shift correlations between the calculated and experimental data.

4. Conclusion

The synthesis of structurally interesting highly functionalized *N*-1-(2-pyridinylmethyl)-3,5-bis[(*E*)-arylmethylidene]tetrahydro-4(1H)-pyridinones have been accomplished in good yield. Structural elucidation of these α,β-unsaturated carbonyl compounds have been carried out through spectroscopic studies and further confirmed by single crystal X-ray diffraction analysis. The different intermolecular contacts control the molecular packing of **5a** and **5b** were predicted quantitatively using Hirshfeld analysis. DFT calculations predicted higher polarity of **5a** than **5b**. The calculated and experimental bond distances and the NMR chemical shifts correlated well. Furthermore, different reactivity indices were also calculated and compared.

Acknowledgements

The authors extend their appreciation to the Deanship of Scientific Research at King Saud University for funding this work through research group no RG-1438-052. This study was also supported by Ondokuz Mayıs University under project No. PYO.FEN.1906.19.001.

Appendix A. Supplementary data

Supplementary data related to this article can be found at…

Credit author statement

Dhaifallah M. Al-thamili: Data curation, Visualization, Investigation

Abdulrahman I. Almansour: Visualization, Investigation and Supervision

Natarajan Arumugam: Visualization, Investigation

Sevgi Kansız: Writing- Reviewing and Editing

Necmi Dege: Visualization, Investigation

Saied M. Soliman: Writing- Original draft preparation

Mohammad Azam: Editing.

Raju Suresh Kumar: Conceptualization, Methodology, Writing- Original draft preparation, Reviewing, Editing and Supervision.

Declaration of interest

The authors declare no conflict of interest.

References

1. A.R. Katritzky, C.A. Ramsden, E.F.V. Screeven, R.J.K. Taylor, Comprehensive Heterocyclic Chemistry III, Elsevier, New York, 2008.
2. T. Eicher, S. Hauptmann, The Chemistry of Heterocycles: Structure, Reactions, Syntheses, and Applications, 2nd ed., Wiley-VCH, Weinheim, 2003
3. F. Lunardi, M. Guzela, A. T. Rodrigues, R. Corre, I. Eger-Mangrich, M. Steindel, Antimicrob. Agents Chemother. 47 (2003) 1449-1451.
4. F. Chimenti, R. Fioravanti, A. Bolasco, P. Chimenti, D. Secci and F. Rossi, J. Med. Chem. 10 (2009) 1-8.

5. A. Zarghi, T. Zebardast, F. Hakimion, F. H. Shirazi, P. N. P. Rao, Bioorg. Med. Chem. 14 (2006) 7044-7050.
6. S. Bag, S. Ramar and M. S. Degani, Med. Chem. Res. 18 (2009) 309-316.
7. A.B. Okey, P.A. Harper, in: H. Galant, D.M. Grant, J. Mitchell (Eds.), Principles of Medical Pharmacology, seventh ed., Elsevier, Toronto, 2007, p. 902.
8. U. Das, H. Sakagami, Q. Chu, Q. Wang, M. Kawase, P. Selvakumar, R.K. Sharma, J.R. Dimmock, Bioorg. Med. Chem. Lett. 20 (2010) 912–917.
9. Y. Santiago-Vazquez, S. Das, U. Das, E. Robles-Escajeda, N.M. Ortega, C. Lema, A. Varela-Ramírez, R.J. Aguilera, J. Balzarini, E. De Clercq, S.G. Dimmock, D.K.J. Gorecki, J.R. Dimmock, Eur. J. Med. Chem. 77 (2014) 315–322.
10. J.R. Dimmock, N.M. Kandepu, A.J. Nazarali, N.L. Motaganahalli, T.P. Kowalchuk, U. Pugazhenthi, J.S. Prisciak, J.W. Quail, T.M. Allen, R. LeClerc, C.L. Santos, E. De Clercq, J. Balzarini, J. Med. Chem. 43 (2000) 3933–3940.
11. J. Sun, S. Zhang, C. Yu, G. Hou, X. Zhang, K. Li, F. Zhao, Chem. Biol. Drug Des. 83 (2014) 392–400.
12. J. Sun, S. Wang, H. Li, W. Jiang, G. Hou, F. Zhao, W. Cong, J. Enzyme Inhib. Med. Chem, 31(2016) 495-502.
13. Y. Kia, H. Osman, R.S. Kumar, V. Murugaiyah, A. Basiri, S. Perumal, H.A. Wahab, C.S. Bing, Bioorg. Med. Chem. 21 (2013) 1696-1707.
14. A. Basiri, V. Murugaiyah, H. Osman, R.S. Kumar, Y. Kia, K.B. Awang, M.A. Ali, Eur. J. Med. Chem. 67 (2013) 221-229.
15. A.I. Almansour, R.S. Kumar, N. Arumugam, D. Sriram, Eur. J. Med. Chem. 53 (2012) 416-423.
16. R.S. Kumar, H. Osman, S. Perumal, J.C. Menéndez, M.A. Ali, R. Ismail, T.S. Choon, Tetrahedron 67 (2011) 3132-3139.
17. R.S. Kumar, S.M. Rajesh, S. Perumal, P. Yogeeswari, D. Sriram, Tetrahedron Assym. 21 (2010) 1315-1327.
18. R.S. Kumar, S. Perumal, H.B. Kagan, R. Guillot, Tetrahedron Assym., 18 (2007) 170-180.
19. R.S. Kumar, A.I. Almansour, N. Arumugam, S.M. Soliman, R.R. Kumar, H.A. Ghabbour, J. Mol. Struc. 1121 (2016) 93-103.

20. R.S. Kumar, A.I. Almansour, N. Arumugam, S.M. Soliman, R.R. Kumar, M. Altaf, H.A. Ghabbour, B.S. Krishnamoorthy, J. Mol. Struc. 1152 (2018) 266-275.
21. Stoe & Cie (2002). *X-AREA* and *X-RED32.* Stoe & Cie, Darmstadt, Germany.
22. G.M. Sheldrick, Acta Cryst. A71 (2015) 3–8.
23. G.M. Sheldrick, Acta Cryst. C71 (2015) 3–8.
24. L.J. Farrugia, J. Appl. Cryst. 32 (1999) 837.
25. C.F. Macrae, P.R. Edgington, P. McCabe, E. Pidcock, G.P. Shields, R. Taylor, M. Towler & J. van de Streek, J. Appl. Cryst. 39 (2006) 453–457.
26. M.J. Turner, J.J. McKinnon, S.K. Wolff, D.J. Grimwood, P.R. Spackman, D. Jayatilaka, M.A. Spackman, Crystal Explorer 17 (2017) University of Western Australia. http://hirshfeldsurface.net
27. M.J. Frisch, G.W. Trucks, H.B. Schlegel, G.E. Scuseria, M.A. Robb, J.R. Cheeseman, G.Scalmani, V.Barone, B.Mennucci, G.A. Petersson, H.Nakatsuji, M. Caricato, X. Li, H.P. Hratchian, A.F. Izmaylov, J.Bloino, G.Zheng, J.L. Sonnenberg, M. Hada, M. Ehara, K. Toyota, R. Fukuda, J. Hasegawa, M. Ishida, T. Nakajima, Y. Honda, O. Kitao, H. Nakai, T. Vreven, J.A. Montgomery, Jr., J.E. Peralta, F. Ogliaro, M. Bearpark, J.J. Heyd, E. Brothers, K.N. Kudin, V.N. Staroverov, R. Kobayashi, J. Normand, K. Raghavachari, A. Rendell, J.C. Burant, S.S. Iyengar, J. Tomasi, M. Cossi, N. Rega, J.M. Millam, M. Klene, J.E. Knox, J.B. Cross, V. Bakken, C. Adamo, J. Jaramillo, R. Gomperts, R.E. Stratmann, O. Yazyev, A.J. Austin, R. Cammi, C. Pomelli, J.W. Ochterski, R.L. Martin, K. Morokuma, V.G. Zakrzewski, G.A. Voth, P. Salvador, J.J. Dannenberg, S. Dapprich, A.D. Daniels, O. Farkas, J.B. Foresman, J.V. Ortiz, J. Cioslowski, D.J. Fox, GAUSSIAN 09. Revision A02. Gaussian Inc., Wallingford CT, USA (2009).
28. GaussView, Version 4.1, R. Dennington II, T. Keith, J. Millam, Semichem Inc., Shawnee Mission, KS, (2007).
29. A.E. Reed, L.A.F. Curtiss, Chem. Rev. 88 (1988) 899–926.
30. B. Marten, K. Kim, C. Cortis, R. A. Friesner, R. B. Murphy, M. N. Ringnalda, D. Sitkoff, B. Honig, J. Phys. Chem. 100 (1996) 11775-11765.
31. D.J. Tannor, B. Marten, R. Murphy, R.A. Friesner, D. Sitkoff, A. Nicholls, M. Ringnalda, W.A. Goddard, B. Honig, J. Am. Chem. Soc. 116 (1994) 11875-11882.

32. J.R. Cheeseman, G.W. Trucks, T.A. Keith, M.J. Frisch, J. Chem. Phys. 104 (1996) 5497-5509.
33. J.R. Dimmock, M.P. Padmanilayam, R.N. Puthucode, A.J. Nazarali, N.L. Motaganahalli, G.A. Zello, J.W. Quail, E.O. Oloo, H.-B. Kraatz, J.S. Prisciak, T.M. Allen, C.L. Santos, J. Balzarini, E. De Clercq, E.K. Manavathu, J. Med. Chem. 44 (2001) 586-593.
34. Crystallographic data have been deposited with the Cambridge Crystallographic Data Centre as supplementary publication number CCDC 1991017 (Compound **5a**) and 1991793 (Compound **5b**). Copies of the data can be obtained free of charge via http://www.ccdc.cam.ac.uk/conts/ retrieving.html, or from the Cambridge Crystallographic Data Centre, 12 Union Road, Cambridge CB2 1EZ, UK. Fax: +44 1223 336033: or e-mail: deposit@ccdc.cam.ac.uk.
35. P. Geerlings, F. De Proft, W. Langenaeker, Chem. Rev. 103 (2003) 1793-1874.
36. L.R. Domingo, M. Ríos-Gutiérrez, P. Pérez, Molecules 21 (2016) 748.
37. J.B. Foresman, A. Frisch, Exploring Chemistry with Electronic Structure Methods, 2nd ed., Gaussian: Pittsburgh, PA, USA, 1996.
38. R. Chang, Chemistry, 7 th ed.; McGraw-Hill: New York, NY, USA, 2001.
39. B. Kosar, C. Albayrak, Spectrochim. Acta-Part. A Mol. Biomol. Spectrosc. 78 (2011) 160–167.
40. T.A. Koopmans, Physica. 1 (1934) 104–113.
41. R.G. Parr, W. Yang, Density Functional Theory of Atoms and Molecules. Oxford University Press: Oxford, UK, 1989.
42. R.G. Parr, L.V. Szentpaly, S. Liu, J. Am. Chem. Soc., 121 (1999) 1922–1924.
43. L.R. Domingo, E. Chamorro, P. Pérez, J. Org. Chem. 73 (2008) 4615-4624.

Graphical abstract

Highly functionalized α,β-unsaturated carbonyl compounds have been achieved in good yields. Structural elucidation was accomplished with the help of NMR spectroscopy and X-ray crystallographic studies. Molecular packing was performed to determine the different intermolecular contacts using Hirshfeld topology analysis. DFT calculations were also performed to evaluate the structural aspects of these compounds.